

SCIENTIFIC REPORTS



OPEN

Enhanced photoelectrochemical aptasensing platform for *TXNDC5* gene based on exciton energy transfer between NCQDs and TiO₂ nanorods

Received: 05 October 2015
Accepted: 08 December 2015
Published: 18 January 2016

Xuehui Pang¹, Lin Wang², Hongmin Ma¹, Yong Zhang¹, Jihong Pan², Yao Chen³, Bin Du¹ & Qin Wei¹

The over expression of thioredoxin domain-containing protein 5 (TXNDC5) can promote the growth of castration-resistant prostate cancer (CRPC). A novel highly sensitive photoelectrochemical (PEC) aptasensor was developed for the detection of TXNDC5 by using the nanohybrids (TiO₂ NRs/NCQDs) of nitrogen-doped carbon quantum dots (NCQDs) and TiO₂ nanorods as the photo-to-electron conversion medium. TiO₂ NRs/NCQDs nanohybrids were prepared by controlling the experimental condition. TiO₂ NRs were self-assembled to form the nanopores with good photocurrent conversion efficiency. NCQDs possessed carboxyl groups (–COOH) and amino groups (–NH₂) in the preparation process. –COOH and –NH₂ groups played important roles for anchoring the capture probes (5' primer and 3' primer) through covalent binding. The ultrasensitive and stable detection for TXNDC5 was achieved by the specific recognition between the capture probes and the targets. The fabricated aptasensor showed excellent performance with a wide linear range (0.5 fmol/L ~ 10 nmol/L) and a low detection limit of 0.1 fmol/L. This kind of aptasensor would provide a potential application for TXNDC5.

Prostate cancer (PCa) is the second leading malignancy in men worldwide in recent years and the incidence has been increasing continuously¹. TXNDC5 is one of the thioredoxin family involved in protein folding and chaperone activity². Aberrant TXNDC5 expression has been reported in multiple malignancies. Therefore the detection of TXNDC5 is very important for the early warning of CRPC. Our group firstly systematically studied the role of TXNDC5 in CRPC³. TXNDC5 expressed at both mRNA and protein levels. However, no work has been done for the detection of TXNDC5. Here, we propose an aptasensor for the detection of the related expressed gene of TXNDC5 based on PEC method. Various PEC aptasensors have been fabricated^{4–7} and PEC method is another promising DNA assay except the traditional electrochemical method^{8–13} due to the low background current and the high sensitivity. The separation of the excitation source and the detection signal makes this method used widely recently^{14–18}. The aptasensor designed in this report will be helpful in the early medical clinical diagnosis.

Compared with the traditional inorganic semiconductor QDs, CQDs have multiple excellent performances^{19–21}. Most importantly, the carbon cores of CQDs are non-toxic and environmentally friendly. No abnormalities are observed in harvested organs although the amounts of CQDs found in liver and spleen are higher than those found in other organs²². These results clearly demonstrate that the CQDs are very desirable as the alternatives to the semiconductor quantum dots^{23,24}. For the field of biosensing, it is very necessary to develop novel CQDs with rich surface functional groups to obtain highly effective and superior biocompatible CQD-based material. At the same time, doping is another widely used method to adjust the properties of CQDs, such as the presence of nitrogen element. N-doping effectively enhances the PEC property of CQDs²⁵.

¹Key Laboratory of Chemical Sensing & Analysis in Universities of Shandong, School of Chemistry and Chemical Engineering, University of Jinan, Jinan 250022, China. ²Shandong Medicinal Biotechnology Centre, the Key Lab for Biotechnology Drugs of Ministry of Health, the Key Lab of Rare and Uncommon Disease, Jinan 250022, China. ³School of Chemistry and Chemical Engineering, Shandong University, Jinan 250100, China. Correspondence and requests for materials should be addressed to Q.W. (email: sdjndxwq@163.com)

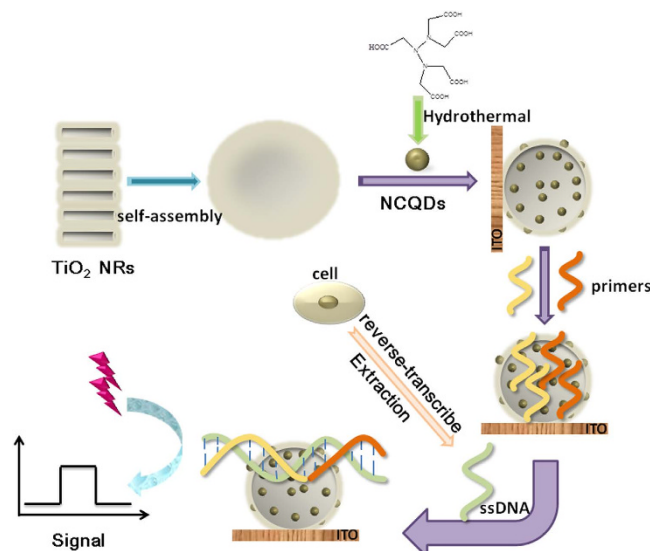


Figure 1. Schematic illustration of the PEC platform fabrication process.

TiO₂ is one of the most studied semiconductor nanostructures^{26–28}. The PEC performance of TiO₂ strongly depends on the dimensionality. Highly oriented TiO₂ single-crystalline NRs grown on the transparent conductive substrates have been considered as the optimum choice of the solar cell materials²⁹. However, a major drawback of TiO₂ NRs is its ineffective utilization of the visible light as the irradiation source. Bandgap engineering by possible modification of TiO₂-based materials is one of the plausible approaches to enhance the performance of TiO₂ NRs, such as QD-sensitized.

Herein, a PEC aptensor based on TiO₂ NRs/NCQDs nanohybrids as the PEC signal medium was constructed (Fig. 1). And the PEC property of TiO₂ NRs/NCQDs was studied under the visible light. This effort offered a promising method for the detections of TXNDC5 or other analytes.

Results and Discussion

Characterizations of TiO₂ NRs, NCQDs, TiO₂ NRs/NCQDs nanohybrids. Scanning electron microscope (SEM) images in Fig. 2A,B showed the morphology of as-prepared TiO₂ NRs. TiO₂ NRs products were assembled as hierarchical microspheres as shown. Figure 2C showed a single magnified broken flower-like microsphere. It can be seen that the microsphere was composed by many uniform TiO₂ NRs with an almost average diameter about 3–5 nm. Figure 2F was EDS result. It showed only Ti, O elements in the sample, which further confirmed the prepared TiO₂ was pure. High resolution transmission electron microscope (HRTEM) was used to reveal the small size of NCQDs (Fig. 2D). HRTEM image showed that the prepared NCQDs had the plentiful output with an average diameter of 3–5 nm. And they were monodisperse nanocrystals of near spherical morphology. Figure 2E showed SEM morphology for TiO₂/NCQDs nanohybrids. TiO₂ NRs and as-assembled microsphere was not rigid and somewhat powder-like attachment can be distinguished on the surface. This suggested that NCQDs hybridized successfully with TiO₂ NRs. EDS result in Fig. 2G showed four elements Ti, O, C, N, which further confirmed the excellent hybridization of TiO₂ NRs and NCQDs.

Figure 3A showed Fourier transform infrared (FT-IR) spectrum of NCQDs in the wavelength range of 500–4000 cm⁻¹. The peak at 1224 cm⁻¹ indicated the characteristic stretch of C–N bond. C=O bending vibration was at 1390 cm⁻¹. The peak of 1625 cm⁻¹ was associated with stretching vibrations of C–O band. The peak at 1730 cm⁻¹ meant C=O stretching vibration. The weak peaks in the range of 2820–3050 cm⁻¹ were related to C–H bond stretching vibrations. A broad peak centered at 3440 cm⁻¹ suggested the presence of many hydroxyl groups on the NCQDs surfaces. All the above mentioned indicated that NCQDs had abundant carboxyl and amino groups on their surfaces. The doped amino and carboxyl groups of NCQDs can increase the hydrophilicity and the combination ability with the detection targets in aqueous systems³⁰.

Figure 3B presented X-ray diffraction (XRD) patterns of NCQDs. A wide peak (002) at about 23° corresponded to an interlayer spacing *d* of 0.385 nm, which agreed with the (002) lattice spacing of carbon-based materials with turbostratic disorder³¹. *d* value was larger than that of graphite (0.34 nm), which indicated that NCQDs possessed abundant oxygen-containing functional groups³². But this *d* value was same to the carbon nanoparticles from pyrolyzing ethanolamine³³ and hydrothermal carbonization of chitosan³⁴.

Figure 3C displayed XRD patterns of TiO₂ NRs, TiO₂/NCQDs. Rutile phase TiO₂ was produced and it can be confirmed by XRD pattern. For TiO₂ NRs, seven diffraction peaks marked (1–7) can be respectively indexed to the (110), (101), (111), (210), (211), (220) and (002) plane. The addition of NCQDs had no obvious influence on the crystallinity and the phase purity of the resultant products. No diffraction peak resulted from NCQDs can be found, which may be attributed to the poor crystallinity and low content³⁵.

PEC performance mechanism proposition. Figure 4A showed time-based photocurrent responses of TiO₂ NRs, TiO₂/NCQDs under the visible light radiation. TiO₂ could be only effectively activated under the light

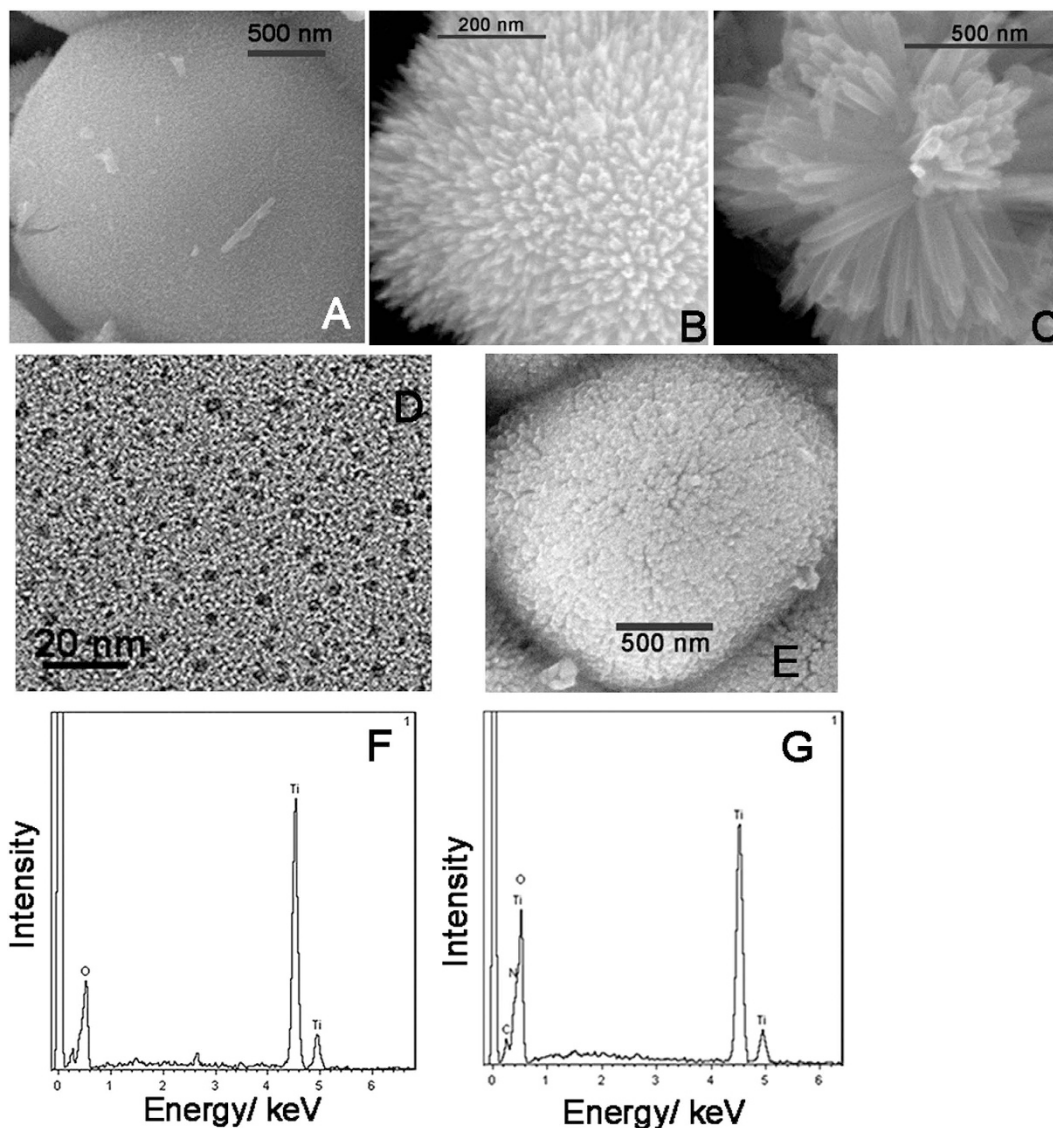


Figure 2. TSEM images of TiO₂ (A–C) and TiO₂/NCQDs nanostructures (E). EM image of NCQDs (D). EDS of TiO₂ (F) and TiO₂/NCQDs nanostructures (G).

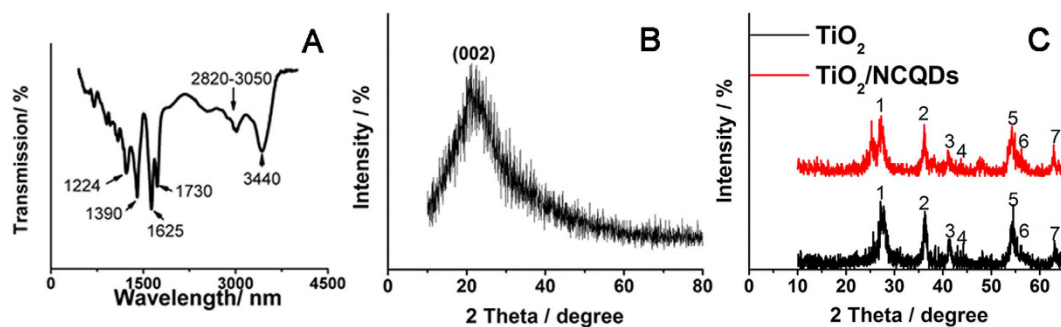


Figure 3. FTIR (A) spectrum of NCQDs. XRD spectrum of NCQDs (B), TiO₂ and TiO₂/NCQDs nanostructures (C).

with short wavelength. The viewpoint was proved by the relatively weak photocurrent response even in the presence of AA in Fig. 4A (a). But the photocurrent of TiO₂/NCQDs were apparently increased about 20 times (b), which proved the addition of NCQDs enhanced PEC behavior. This might be explained that h⁺/e⁻ pair separation efficiency was distinctly enhanced through the electron injection between NCQDs and TiO₂ NRs.

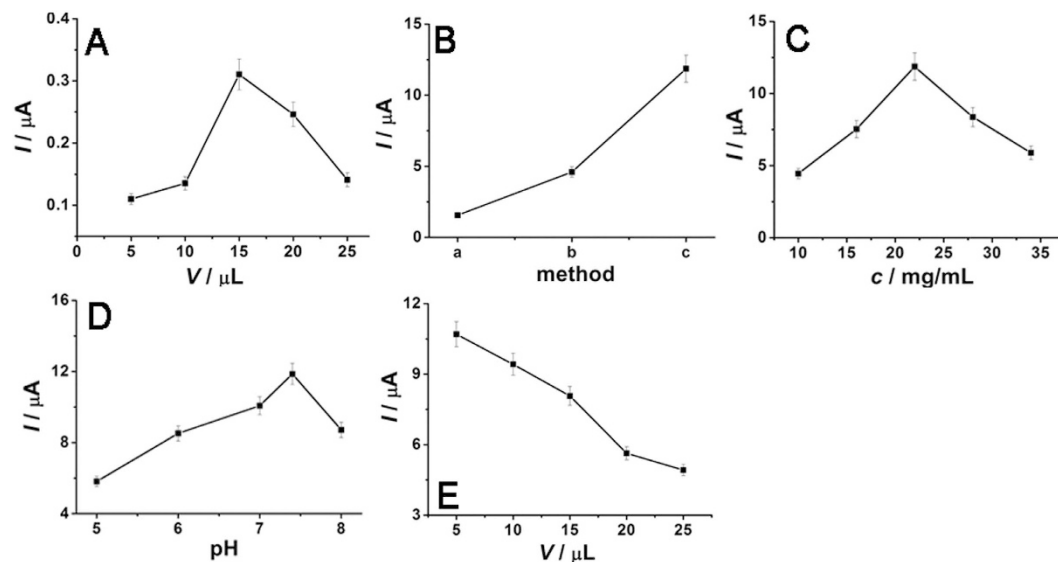


Figure 6. The optimization of experimental conditions by time-based photocurrent response of (A) different application amount of TiO₂ NRs on ITO electrode (pH = 7.4), (B) different composition methods (a for method 1, b for method 2 and c for method 3) of TiO₂ NRs and NCQDs, (C) different application amount of NCQDs in the composition process in the method 1, (D) different pH after modifying 10 μL of TiO₂/NCQDs nano hybrids, (E) different application amount of 3' and 5' primers after modifying 10 μL of TiO₂/NCQDs nano hybrids (pH = 7.4).

The relative Fermi level alignment of rutile TiO₂ and NCQDs were shown in Fig. 5. The band gap of TiO₂ NRs was 3.2 eV³⁶ and the CB energy level was -0.44 V (vs. normal hydrogen electrode, NHE)⁴¹. Then the VB energy level of TiO₂ NRs can be deduced about 2.76 V (according to $E_g = V_{VB} - V_{CB}$). The band gap of NCQDs was about 1.9 eV⁴², the VB energy level was about 0 V⁴³. So the CB energy level was about -1.9 V . Under the visible light, NCQDs absorbed the visible and near-infrared light, and then converted them to shorter wavelengths due to the up-converted property^{44,45}. The shorter wavelengths that less than or equal to 380 nm can excite TiO₂ NRs to produce the e^-/h^+ pairs. NCQDs can accept the photogenerated electrons from TiO₂ NRs and promote the separation of the photogenerated e^-/h^+ pairs.

Thus, from the schematic diagram of the process, it can be seen that the VB and CB energy levels of NCQDs lied above those of TiO₂ NRs. Under the visible light irradiation, the electrons in the VB of NCQDs obtained enough energy and injected to the CB. The photogenerated electrons can be easily injected from NCQDs into TiO₂ NRs *via* the interface injection. However, the holes on the VB of TiO₂ NR scan transfer to NCQDs. As a reducing agent, AA acted as an electron donor to trap the holes in the VB of TiO₂, which inhibited the e^-/h^+ recombination and improved the photocurrent response⁴⁶. After that, the electrons were transported through ITO film and conducted through the external circuit to the counter electrode.

Therefore, NCQDs in the nanocomposites facilitated the transfer of the electrons from TiO₂ NRs and the electrons can be shuttled freely along the conducting paths in NCQDs. The combination of TiO₂ NRs/NCQDs benefited for the charge separation and for hindering e^-/h^+ recombination^{47,48}. And what's more, N-doping was another main reason for the enhancement of the photocatalytic activity of TiO₂/NCQDs. N-doping can lower the work function of carbon nanomaterials and the lower work function of NCQDs produced much smaller barrier between NCQDs and TiO₂. The inference was also proved by UV-vis and PL measurement as shown in Fig. 4B,C. The above results illuminated that NCQDs can help for the transfer of the photogenerated electrons and reduce the recombination rate of e^-/h^+ pairs.

Characterizations of the fabricated PEC aptensor. In order to realize better detecting effect, the optimization of the experimental conditions was carried out. The application amount of TiO₂ NRs, the composition methods (three methods) of TiO₂ NRs and NCQDs, the application amount of NCQDs composited with TiO₂ NRs, pH values and the application amount of 3' and 5' primers were investigated in this study (Fig. 6). The obtained optimum experimental conditions were the application amount of TiO₂ NRs = 15 μL (Fig. 6A), the composition method was method 1 (Fig. 6B), the application amount of NCQDs = 22 mg/mL (Fig. 6C), pH = 7.4 (Fig. 6D) and the application amount of 3' and 5' primers = 15 μL (Fig. 6E), respectively.

The fabrication procedure of the PEC aptensor could also be monitored by the photocurrent responses under the optimal experimental condition (Fig. 7A). PB solution contained 0.1 mol/L of AA to improve photocurrent conversion efficiency. Curve a showed there was almost non photocurrent response for bare ITO electrode. The photocurrent remarkably enhanced when TiO₂/NCQDs nano hybrids were modified on ITO electrode (curve b). This indicated that the composition of NCQDs with TiO₂ NRs conspicuously increased the photocurrent. Because of the composition of NCQDs and TiO₂ NRs, the electron transfer efficiency enhanced much and the recombination probability between the electrons and the holes was depressed apparently. And also the composition manner

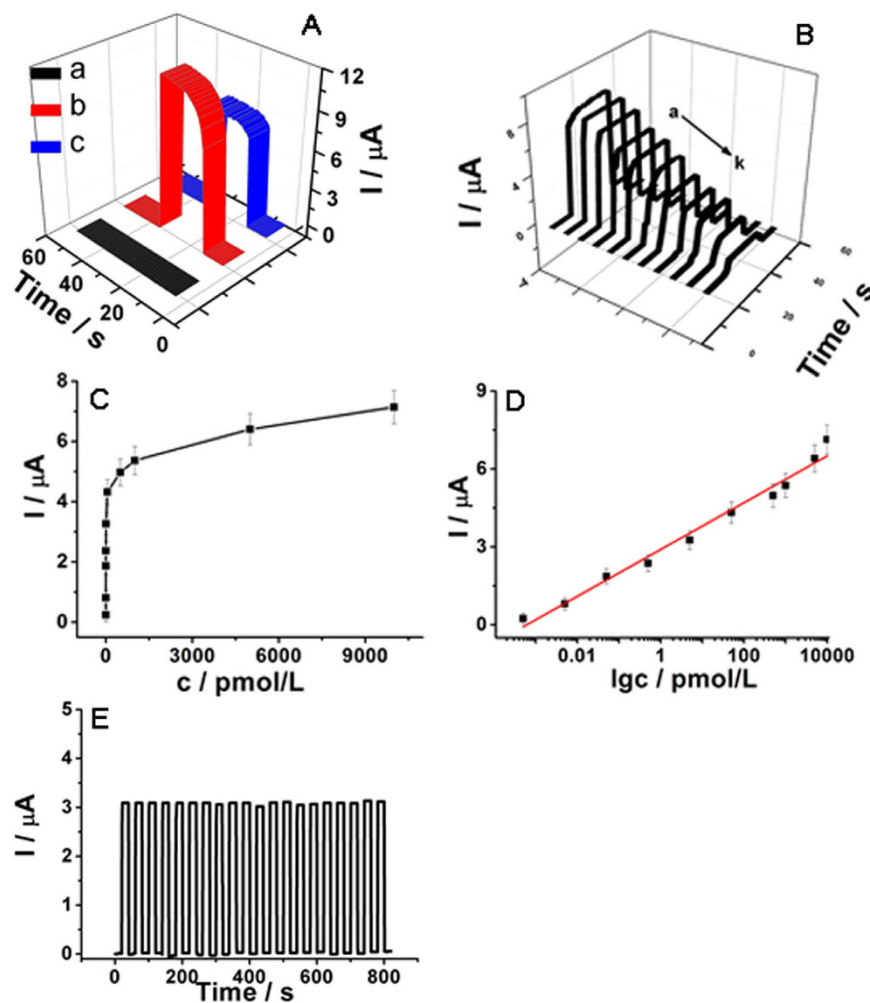


Figure 7. (A) Time-based photocurrent responses of: (a) naked ITO, (b) after modifying with TiO₂/NCQDs nano hybrids, (c) after anchoring the primers. (B) Time-based photocurrent response of the aptensor incubated with different concentration of TXNDC5; (C) Relation curve between photocurrent change (ΔI) and different TXNDC5 concentrations; (D) Logarithmic calibration curve between ΔI and c_{TXNDC5} ; (E) Stability of photocurrent response under the optimal conditions.

was also investigated (Fig. 6B). TiO₂/NCQDs prepared by method 2 showed poor PEC property with a photocurrent about 1.5 μA . TiO₂/NCQDs prepared by method 3 displayed better PEC performance with a photocurrent about 4.6 μA . Only method 1 can make the photocurrent of TiO₂/NCQDs improve obviously up to about 11.9 μA . The temperature and duration time using in method 1 might result in the effective combination between TiO₂ and NCQDs. This effective combination might make the electrons injection much easier between CB and VB. Later on, when the primers of TXNDC5 were modified on the electrode, the photocurrent reduced (curve c). The bases of the primers owned $-\text{NH}_2$ groups and TiO₂/NCQDs have $-\text{COOH}$ groups. When the primers were incubated on the modified ITO electrode surface, the interaction between the amino groups of primers and the carboxyl group of TiO₂/NCQDs would occur under the activation of EDC/NHS amidization protocol. TiO₂/NCQDs can immobilize the primers probes on ITO electrode through the interaction. But the bases can not transfer the electrons and absorb the visible light, which would result in the obstruction of the absorption of the light and the suppression of the electrons transfer. This would cause the decrease of the photocurrent and the experimental results proved this speculation. Therefore, the PEC aptensor was fabricated as expected.

Analytical performance characteristics. In order to investigate the possibility of the aptensor applied for TXNDC5 analysis, quantitative detection of TXNDC5 was operated under the optimal conditions. The process began after incubating various concentrations of TXNDC5 on ITO electrode. The detection results were given in Fig. 7B,C. The concentration of TXNDC5 affected the strength of the photocurrent response and a stronger response was achieved at high TXNDC5 concentration. This indicated that the proposed PEC platform showed good detection performance so that it can be used for the TXNDC5 quantitative detection. A calibration graph was plotted under the optimal conditions (Fig. 7D). A positive relationship can be deduced between the photocurrent response signal change and the target concentration. PEC signal change increased linearly with the logarithm of the TXNDC5 concentration from 0.5 fmol/L to 10.0 nmol/L. The linear equation was obtained as ΔI

(μA) = $2.901 + 0.901 \lg c_{\text{TXNDC5}}$ (pmol/L) and the correlation coefficient was 0.991. A detection limit of 0.1 fmol/L was obtained for the reported aptsensor. The proposed PEC aptsensor therefore showed a wide linear range and a low detection limit for the determination of TXNDC5. The low detection limit may be ascribed to good separated excitation energy of $\text{TiO}_2/\text{NCQDs}$ and the specific recognition between the capture probe and the target.

Stability and reproducibility were two important parameters affecting the practical application of an aptsensor. Figure 7E showed the photocurrent responses of the PEC aptsensor with the visible-light irradiation repeated every 20 s. The irradiation process was repeated 20 on/off cycles over 800 s. During every on/off cycle, the photocurrent did not show any obvious change. This indicated that the photocurrent response was very stable and this strategy was appropriate to construct the PEC sensors. A series of six electrodes were fabricated and used to determinate 500 pmol/L of TXNDC5. All of the tests were carried out under the same conditions. The relative standard deviation (RSD) for TXNDC5 was 1.8%, so the reproducibility of the proposed PEC aptsensor was good.

Conclusions

This work proposed a novel PEC aptsensor for the rapid and ultrasensitive detection of TXNDC5. The specific detection was realized by specific recognition between the capture probe and the target. When exposed to the visible light, the signal generator of TiO_2 NRs/NCQDs nanohybrids expressed significantly enhanced PEC property. The combination of NCQDs improved the charge separation efficiency and the charge transfer ability, and suppressed the h^+/e^- recombination effectively. The developed aptsensor displayed the ultra-sensitivity and good stability. Thus, it provided good detection effect for TXNDC5 and might provide a feasible platform to determinate of other analyses.

Methods

Regents. Phosphate buffered solution (PB, 0.067 mol/L KH_2PO_4 and 0.067 mol/L Na_2HPO_4) were used as the electrolyte for all electrochemistry measurements. All other chemical reagents were analytical reagent grade and directly used without further purification. The ultrapure water (resistivity of 18.25 $\text{M}\Omega\cdot\text{cm}$) and pipette tips were put into a LDZX-30KBS pressure steam sterilizer (Shanghai Shenan Medical Instrument) and sterilized at 121 °C for 40 min. After cooling to room temperature, the tips were stored in a 4 °C refrigerator.

Apparatus. SEM images were obtained from JSM-6700F microscope (JEOL, Japan). HRTEM image was recorded by JEM-2100F microscope (JEOL, Japan). FT-IR spectra were obtained with Perkin-Elmer 580B spectrophotometer (Perkin-Elmer, USA). XRD patterns were collected from D8 focus diffractometer (Bruker AXS, Germany). PEC tests were carried out on electrochemical work station (Zahner Zennium PP211, Germany). UV-vis measurements were obtained on Lambda 35 UV-vis spectrometer (Perkin-Elmer, USA). PL spectra were obtained on LS-45/55 PL spectrometer (Perkin-Elmer, USA).

Preparation of TXNDC5. TXNDC5 was prepared according to our previous work³. TXNDC5 mRNA was reverse-transcribed by ReverTra Ace qPCR RT kit and SYBR Green PCR kit (Toyobo, Osaka, Japan). The primers for the amplification of TXNDC5 were as follows: forward primer 5'-CTC TGG GCC TTG AAC ATT-3' and reverse primer 5'-CCC TCA GTG ACT CCA AA-3'. The sequence of TXNDC5 was as follows: 5'-CTC TGG GCC TTG AAC ATT CCG AAA CTG TCA AGA TTG GCA AGG TTG ATT GTA CAC AGC ACT ATG AAC TCT GCT CCG GAA ACC AGG TTC GTG GCT ATC CCA CTC TTC TCT GGT TCC GAG ATG GGA AAA AGG TGG ATC AGT ACA AGG GAA AGC GGG ATT TGG AGT CAC TGA GGG-3'. The specificity of the qRT-PCR assay was evaluated by melting curve analysis. It showed that the TXNDC5 amplification product generated a melting peak at 81.20 ± 0.34 °C without primer-dimers or nonspecific products. 15 μL of 5' primer (10 $\mu\text{mol/L}$) and 15 μL of 3' primer (10 $\mu\text{mol/L}$) were diluted respectively with 323 μL ultrapure water (0 °C). Then the mixtures were oscillated for 40 min under 0 °C. The concentration of the diluted primers was much greater than that of TXNDC5.

Preparation of TiO_2 NRs. TiO_2 NRs were prepared according to the method in the literature with slight modifications³⁵. 5 g of TiCl_3 aqueous solution and 4 g of NaCl were added into 10 mL of distilled water under stirring. The solution was put into a Teflon-lined stainless steel autoclave with a capacity of 50 mL. The autoclave was sealed and heated at 100 °C for 12 h. After cooling to room temperature, the products were washed with distilled water and absolute ethanol for several times. Then the products dried under vacuum for use.

Preparation of NCQDs. NCQDs were prepared as the method described in the literature with slight modifications³⁰. 2 g of DTPA was placed in 20 mL ultrapure water and stirred vigorously to form a turbid liquid. Then, the formed liquid turned into the colorless solution by heating. The heating process (100 °C) was continued until the colorless solution became a yellow clustered solid, indicating the formation of NCQDs. The yellow solid was dissolved in 20 mL ultrapure water. After that, the yellow crude NCQDs solution was centrifuged at 8000 r/min for 15 min to remove the unreacted DTPA. Finally, the obtained supernatant was freeze-dried to get the pure solid of NCQDs.

Preparation of TiO_2 NRs/NCQDs. Method 1: TiO_2 NRs/NCQDs nanohybrids were prepared as described in the literature with slight modifications³⁵. 5 g of TiCl_3 aqueous solution, 4 g of NaCl and 10 ~ 28 mg of NCQDs powder were added into 10 mL of distilled water under stirring. The following procedure was same to the preparation of TiO_2 NRs. TiO_2 NRs/NCQDs nanohybrids were prepared as method 2, 3 (ESI†).

Fabrication of the PEC aptsensor. The fabrication procedure of the PEC aptsensor was shown in Fig. 1. Firstly, ITO conductive glass was cut (1.0 cm \times 2.5 cm, rectangle) as the working electrode, washed orderly by ultrasonication for 30 min with acetone, ethanol and ultrapure water respectively, and dried by pure nitrogen.

Secondly, 10 μL of $\text{TiO}_2/\text{NCQDs}$ nanohybrids were dropped on ITO electrode and dried in a 4 °C refrigerator. Thirdly, 15 μL of diluted 5' primer was dropped on $\text{TiO}_2/\text{NCQDs}/\text{ITO}$ electrode surface using an EDC/NHS amidization protocol and incubated in a 4 °C refrigerator for 4 h. After that, 15 μL of 3' primer was dropped on 5' primer/ $\text{TiO}_2/\text{NCQDs}/\text{ITO}$ electrode using an EDC/NHS amidization protocol and incubated in a 4 °C refrigerator for 4 h. At last, TXNDC5 ssDNA with different concentrations were dropped on 3' primer/5' primer/ $\text{TiO}_2/\text{NCQDs}/\text{ITO}$ electrode surface respectively and incubated at 4 °C for 4 h.

Measurement procedure. The PEC measurements were performed immediately after the incubation of TXNDC5 ssDNA. A conventional three-electrode system was used in all the PEC experiments. A platinum wire was the auxiliary electrode. A KCl-saturated calomel electrode (SCE) was the reference electrode. The modified ITO electrode was used as the working electrode. A commercial LED light (430 nm) was used as the irradiation energy in all the PEC tests. PB containing 0.1 mol/L of ascorbic acid (AA) was used as an electrolyte solution for all the PEC measurements. The bias voltage was 0.1 V. Both light duration and no light duration were 20 s. All the PEC experiments were operated at room temperature.

References

- Zhao, L. *et al.* Tissue biomarkers for prognosis of prostate cancer: A systematic review and meta-analysis. *Cancer Epidem. Biomar.* **23**, 1047–1054 (2014).
- Gulerez, I. E., Kozlov, G., Rosenauer, A. & Gehring, K. Structure of the third catalytic domain of the protein disulfide isomerase ERp46. *Acta Crystallogr.* **F68**, 378–381 (2012).
- Wang, L. *et al.* The role of TXNDC5 in castration-resistant prostate cancer-involvement of androgen receptor signaling pathway. *Oncogene*. 1–11 (2014).
- Xia, L. *et al.* CdS quantum dots modified CuO inverse opal electrodes for ultrasensitive electrochemical and photoelectrochemical biosensor. *Sci. Rep.* **5**, 10838 (2015).
- Fan, G. C., Ren, X. L., Zhu, C., Zhang, J. R. & Zhu, J. J. A new signal amplification strategy of photoelectrochemical immunoassay for highly sensitive interleukin-6 detection based on $\text{TiO}_2/\text{CdS}/\text{CdSe}$ dual co-sensitized structure. *Biosens. Bioelectron.* **59**, 45–53 (2014).
- Chen, D., Zhang, H., Li, X. & Li, J. Biofunctional titania nanotubes for visible-light-activated photoelectrochemical biosensing. *Anal. Chem.* **82**, 2253–2261 (2010).
- Tu, W., Dong, Y., Lei, J. & Ju, H. Low-potential photoelectrochemical biosensing using porphyrin-functionalized TiO_2 nanoparticles. *Anal. Chem.* **82**, 8711–8716 (2010).
- Peng, F. *et al.* Silicon nanomaterials platform for bioimaging, biosensing, and cancer therapy. *Acc. Chem. Res.* **47**, 612–623 (2014).
- Liu, H. *et al.* An amplified electrochemical strategy using DNA-QDs dendrimer superstructure for the detection of thymine DNA glycosylase activity. *Biosens. Bioelectron.* **71**, 249–255 (2015).
- Yang, G., Li, L., Rana, R. K. & Zhu, J. Assembled gold nanoparticles on nitrogen-doped graphene for ultrasensitive electrochemical detection of matrix metalloproteinase-2. *Carbon* **61**, 357–366 (2013).
- Hu, L., Tan, T., Chen, G., Zhang, K. & Zhu, J.-J. Ultrasensitive electrochemical detection of BCR/ABL fusion gene fragment based on polymerase assisted multiplication coupling with quantum dot tagging. *Electrochem. Commun.* **35**, 104–107 (2013).
- Yang, Y. *et al.* An electrochemically actuated reversible DNA switch. *Nano. Lett.* **10**, 1393–1397 (2010).
- Zhu, C. *et al.* Single-layer MoS_2 -based nanoprobe for homogeneous detection of biomolecules. *J. Am. Chem. Soc.* **135**, 5998–6001 (2013).
- Ma, W. *et al.* Biomolecule-free, selective detection of *o*-diphenol and its derivatives with WS_2/TiO_2 -based photoelectrochemical platform. *Anal. Chem.* **87**, 4844–4850 (2015).
- Shen, Q. *et al.* "Signal-On" photoelectrochemical biosensor for sensitive detection of human T-cell lymphotropic virus type II DNA: Dual signal amplification strategy integrating enzymatic amplification with terminal deoxynucleotidyl transferase-mediated extension. *Anal. Chem.* **87**, 4949–4956 (2015).
- Wang, G. *et al.* Using G-Quadruplex/hemin to "switch-on" the cathodic photocurrent of *p*-Type PbS quantum dots: Toward a versatile platform for photoelectrochemical aptasensing. *Anal. Chem.* **87**, 2892–2900 (2015).
- Zang, Y., Lei, J., Ling, P. & Ju, H. Catalytic hairpin assembly-programmed porphyrin–DNA complex as photoelectrochemical Initiator for DNA biosensing. *Anal. Chem.* **87**, 5430–5436 (2015).
- Zhao, W., Wang, J., Zhu, Y., Xu, J. & Chen, H. Quantum dots: Electrochemiluminescent and photoelectrochemical bioanalysis. *Anal. Chem.* **87**, 9520–9531 (2015).
- Ananthanarayanan, A. *et al.* Facile synthesis of graphene quantum dots from 3D graphene and their application for Fe^{3+} sensing. *Adv. Funct. Mater.* **24**, 3021–3026 (2014).
- Barman, S. & Sadhukhan, M. Facile bulk production of highly blue fluorescent graphitic carbon nitride quantum dots and their application as highly selective and sensitive sensors for the detection of mercuric and iodide ions in aqueous media. *J. Mater. Chem.* **22**, 21832–21837 (2012).
- Dong, Y. *et al.* Polyamine-functionalized carbon quantum dots as fluorescent probes for selective and sensitive detection of copper ions. *Anal. Chem.* **84**, 6220–6224 (2012).
- Yang, S. *et al.* Carbon dots as nontoxic and high-performance fluorescence imaging agents. *J. Phys. Chem.* **C113**, 18110–18114 (2009).
- Bourlinos, A. B. *et al.* Photoluminescent carbogenic dots. *Chem. Mater.* **20**, 4539–4541 (2008).
- Baker, S. N. & Baker, G. A. Luminescent carbon nanodots: emergent nanolights. *Angew. Chem. Int. Edit.* **49**, 6726–6744 (2010).
- Ayala, P., Arenal, R., Loiseau, A., Rubio, A. & Pichler, T. The physical and chemical properties of heteronanotubes. *Rev. Mod. Phys.* **82**, 1843 (2010).
- Yin, Y. & Talapin, D. The chemistry of functional nanomaterials. *Chem. Soc. Rev.* **42**, 2484–2487 (2013).
- Chen, X. & Mao, S. S. Titanium dioxide nanomaterials: synthesis, properties, modifications, and applications. *Chem. Rev.* **107**, 2891–2959 (2007).
- Chen, J., Yang, H. B., Miao, J., Wang, H. Y. & Liu, B. Thermodynamically driven one-dimensional evolution of anatase TiO_2 nanorods: one-step hydrothermal synthesis for emerging intrinsic superiority of dimensionality. *J. Am. Chem. Soc.* **136**, 15310–15318 (2014).
- Jennings, J. R., Ghicov, A., Peter, L. M., Schmuki, P. & Walker, A. B. Dye-sensitized solar cells based on oriented TiO_2 nanotube arrays: transport, trapping, and transfer of electrons. *J. Am. Chem. Soc.* **130**, 13364–13372 (2008).
- Han, T. *et al.* Eco-friendly synthesis of electrochemiluminescent nitrogen-doped carbon quantum dots from diethylene triamine pentacetate and their application for protein detection. *Carbon* **91**, 144–152 (2015).
- Liu, Y., Xue, J., Zheng, T. & Dahn, J. Mechanism of lithium insertion in hard carbons prepared by pyrolysis of epoxy resins. *Carbon* **34**, 193–200 (1996).
- Peng, J. *et al.* Graphene quantum dots derived from carbon fibers. *Nano. Lett.* **12**, 844–849 (2012).

33. Dong, X. *et al.* Fast one-step synthesis of N-doped carbon dots by pyrolyzing ethanolamine. *J. Mater. Chem.* **C2**, 7477–7481 (2014).
34. Yang, Y. *et al.* One-step synthesis of amino-functionalized fluorescent carbon nanoparticles by hydrothermal carbonization of chitosan. *Chem. Commun.* **48**, 380–382 (2012).
35. Zhang, Y., Ma, D., Zhang, Y., Chen, W. & Huang, S. N-doped carbon quantum dots for TiO₂-based photocatalysts and dye-sensitized solar cells. *Nano Energy* **2**, 545–552 (2013).
36. Huang, Q. *et al.* Enhanced photocatalytic activity of chemically bonded TiO₂/graphene composites based on the effective interfacial charge transfer through the C-Ti Bond. *ACS Catal.* **3**, 1477–1485 (2013).
37. Pan, D. *et al.* Observation of pH-, solvent-, spin-, and excitation-dependent blue photoluminescence from carbon nanoparticles. *Chem. Commun.* **46**, 3681–3683 (2010).
38. Cheng, C. *et al.* Enhanced photocatalytic performance of TiO₂-ZnO hybrid nanostructures. *Scientific reports* **4**, 4181 (2014).
39. Dimitrijevic, N. M., Saponjic, Z. V., Rabatic, B. M. & Rajh, T. Assembly and charge transfer in hybrid TiO₂ architectures using biotin-avidin as a connector. *J. Am. Chem. Soc.* **127**, 1344–1345 (2005).
40. Zhao, W., Ma, Z., Xu, J. & Chen, H. In situ modification of a semiconductor surface by an enzymatic process: A general strategy for photoelectrochemical bioanalysis. *Anal. Chem.* **85**, 8503–8506 (2013).
41. Kanan, M. W. & Nocera, D. G. In situ formation of an oxygen-evolving catalyst in neutral water containing phosphate and Co²⁺. *Science* **321**, 1072–1075 (2008).
42. Sun, M. *et al.* A nanocomposite of carbon quantum dots and TiO₂ nanotube arrays: enhancing photoelectrochemical and photocatalytic properties. *RSC Adv.* **4**, 1120–1127 (2014).
43. Narayanan, R., Deepa, M. & Srivastava, A. K. Förster resonance energy transfer and carbon dots enhance light harvesting in a solid-state quantum dot solar cell. *J. Mater. Chem.* **A1**, 3907 (2013).
44. Zhang, H. *et al.* Carbon quantum dots/Ag₃PO₄ complex photocatalysts with enhanced photocatalytic activity and stability under visible light. *J. Mater. Chem.* **22**, 10501–10506 (2012).
45. Yu, X., Liu, J., Yu, Y., Zuo, S. & Li, B. Preparation and visible light photocatalytic activity of carbon quantum dots/TiO₂ nanosheet composites. *Carbon* **68**, 718–724 (2014).
46. Gao, P. *et al.* Anatase TiO₂ based photoelectrochemical sensor for the sensitive determination of dopamine under visible light irradiation. *New J. Chem.* **39**, 1483–1487 (2015).
47. Yao, Y., Li, G., Ciston, S., Lueptow, R. M. & Gray, K. A. Photoreactive TiO₂/carbon nanotube composites: synthesis and reactivity. *Environ. Sci. Technol.* **42**, 4952–4957 (2008).
48. Lim, S. Y., Shen, W. & Gao, Z. Carbon quantum dots and their applications. *Chem. Soc. Rev.* **44**, 362–381 (2015).

Acknowledgements

This research was supported by National Natural Science Foundation of China (Nos. 21175057, 21375047, 21377046, 21405059, 21575050, 21505051), the Science and Technology Development Plan of Shandong Province (No. 2014GSF120004), the Special Project for Independent Innovation and Achievements Transformation of Shandong Province (No. 2014ZZCX05101), the Technology Research Project of Shandong Provincial Education Department (J15LC07), Taishan Scholar Professorship of Shandong Province and UJN (No. ts20130937).

Author Contributions

X.P. and Y.Z. wrote the manuscript; Q.W. and H.M. conceived the idea; L.W., Y.Z. and J.P. carried out the preparation of the bio-specimens; X.P., Y.C. and B.D. carried out the measurement and analyzed data. All authors reviewed the manuscript.

Additional Information

Supplementary information accompanies this paper at <http://www.nature.com/srep>

Competing financial interests: The authors declare no competing financial interests.

How to cite this article: Pang, X. *et al.* Enhanced photoelectrochemical aptasensing platform for *TXNDC5* gene based on exciton energy transfer between NCQDs and TiO₂ nanorods. *Sci. Rep.* **6**, 19202; doi: 10.1038/srep19202 (2016).



This work is licensed under a Creative Commons Attribution 4.0 International License. The images or other third party material in this article are included in the article's Creative Commons license, unless indicated otherwise in the credit line; if the material is not included under the Creative Commons license, users will need to obtain permission from the license holder to reproduce the material. To view a copy of this license, visit <http://creativecommons.org/licenses/by/4.0/>